J. Fluid Mech. (1978), *vol.* 86, *part* 3, *pp.* 545–566
Printed in Great Britain

Measurements of turbulent flow downstream of a rearward-facing step

By D. W. ETHERIDGE† AND P. H. KEMP
Department of Civil and Municipal Engineering, University College London

(Received 14 April 1976 and in revised form 27 September 1977)

Measurements have been made in a water channel of the flow in and around the separation region due to a rearward-facing step. Detailed profiles of mean velocities, turbulence intensities and Reynolds shear stress are presented. The turbulence measurements reveal the development of a new shear layer, which splits at reattachment with about one-sixth of the mass flow deflected upstream. The new shear layer is associated with a region of roughly constant values of both the non-dimensional mixing length l/x and the shear correlation coefficient K. The mixing-length ratio is larger than that found in plane mixing layers, whereas the shear coefficient is roughly the same. There is strong evidence that near the wall the length scales increase more rapidly with distance from the wall than in an attached boundary layer, and that a local maximum occurs.

1. Introduction

The work described here is the basis of a continuing investigation of the influence of flow separation on phenomena such as sediment transport and bed forms which are encountered in rivers and estuaries. A simple step was chosen, first because it serves as a convenient reference for more complex bed forms and second because it is representative of features such as man-made structures which are associated with a wide range of problems in fluid mechanics.

A laser anemometer was developed for the work since conventional anemometers impose severe limitations on the measurement of separated flows.

As the work proceeded it became apparent that the results were considerably different to those obtained in earlier studies and so it was extended to obtain detailed information on the flow both in and around the separation region. Examples of the differences between the present results and earlier ones can be seen in figure 1. Here the profiles of $\bar{u}/\bar{u}_{\max}$, $(\overline{u'^2})^{\frac{1}{2}}/\bar{u}_{\max}$, $(\overline{v'^2})^{\frac{1}{2}}/\bar{u}_{\max}$ and $-\overline{u'v'}/\bar{u}^2_{\max}$ at one streamwise station ($x/H_s = 4{\cdot}0$) measured by Walker and described by Raudkivi (1963) are compared with the present results (the notation is given below). Walker used a channel which is similar to the present one, but his measurements were made with a hot film and this almost certainly explains the bulk of the differences which are clearly evident. Support for this can be seen in figure 2, where a similar comparison is made with the recent results of Grant, Barnes & Greated (1975), who used a laser system. Although their results are much less detailed than the present ones it can be seen that the agreement is much closer.

† Present address: British Gas Corporation, Watson House, Peterborough Road, London SW6.

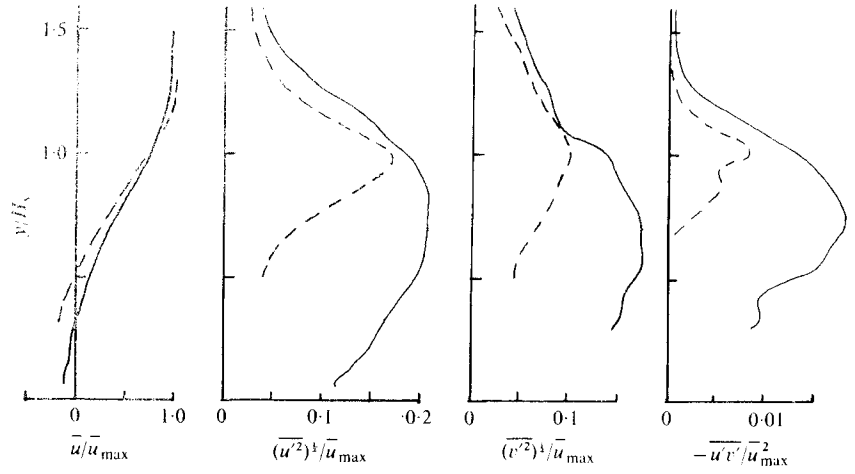

FIGURE 1. Comparison between present results (solid curves) and those of Walker (dashed curves) at $x/H_s = 4{\cdot}0$.

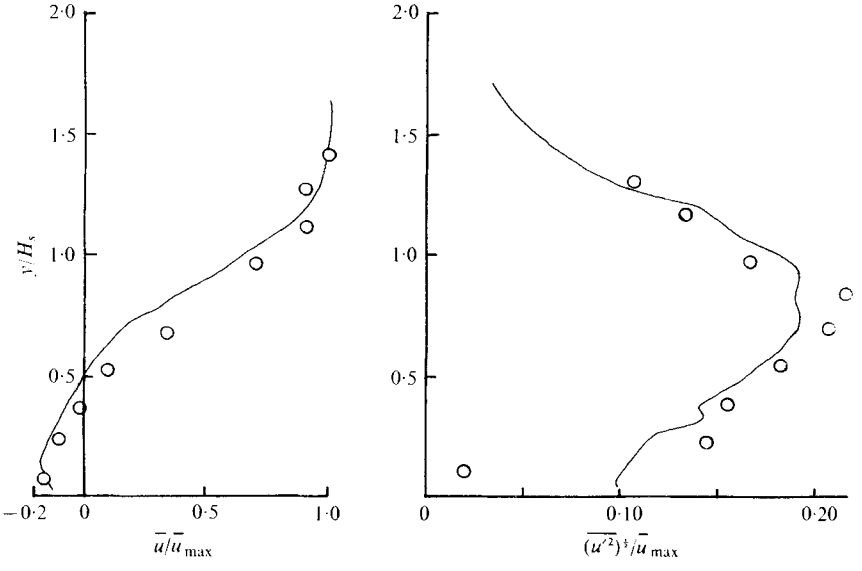

FIGURE 2. Comparison between present results (solid curves) and those of Grant *et al.* (circles) at $x/H_s = 3{\cdot}0$.

2. Experimental equipment and technique

2.1. *Channel*

The measurements were made in a recirculating-flow water channel of width 150 mm with a water depth of 200 mm. A rearward-facing step with a height H_s of 13·46 mm was situated 750 mm from the entrance to the channel. The channel is preceded by a settling tank, which is supplied by a constant-head tank. The settling tank is equipped with a honeycomb, four meshes and an inlet fairing with a contraction ratio of 19.

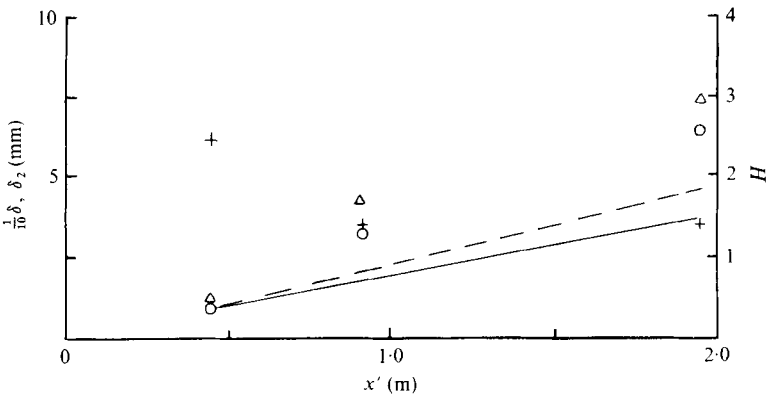

FIGURE 3. Measured development of the momentum thickness δ_2 (circles), boundary-layer thickness δ (triangles) and shape parameter H (crosses). ——, growth of δ_2 attributable to skin friction; – – –, with convergence.

At the outset it was appreciated that the channel was rather narrow and that to minimize departures from flow two-dimensionality the step would have to be placed quite near the channel entrance. The streamwise position x'_s of the step and the step height H_s were chosen on the basis of two preliminary investigations of the channel flow.

The aim of the first investigation was to measure the boundary-layer development along the centre-line of the channel so as to gain an idea of its form and thickness and an indication of the effect of the side-wall boundary-layer growth. Profiles of the streamwise mean velocity $\bar{u}$ and turbulence levels were measured at three streamwise stations ($x' = 0{\cdot}44$, $0{\cdot}91$ and $1{\cdot}94$ m, where x' denotes distance from the channel entrance). Figure 3 shows the development of the momentum thickness δ_2, the shape parameter H and the approximate thickness δ. The development of δ_2 is compared with the growth attibutable to skin friction. This has been obtained by making use of the Ludwieg–Tillman relation (quoted below). It is clear that the growth is not solely due to skin friction. An attempt was made to account for the greater growth by assuming that the centre-line was a line of flow symmetry and estimating the extra growth due to linear convergence of the streamlines at the outer edge of the boundary layer. As can be seen in the figure, this goes some way towards accounting for the larger growth. However the velocity measurements showed that the external flow was accelerating and, when this was allowed for, most of the extra growth due to convergence was counteracted. The increased growth could be due to a spanwise (i.e. cross-flow) velocity component in the flow arising from curvature of the external streamlines, but it was not possible to estimate this from the measurements.

As a result of the above investigation it was decided to use a step of height about 13 mm and to position it at $x' = 0{\cdot}75$ m. It was also decided to investigate directly the two-dimensionality of the flow upstream of the step. The choice of step height was a compromise between having a sufficiently large step to give a strong flow perturbation and to allow detailed measurements in the separated region and maintaining a large ratio of channel width to step height. At the chosen position δ/H_s is about 2, so that the flow is strongly perturbed by the step. The influence of the upstream boundary layer could not be neglected, however, and so it was decided to place the step further

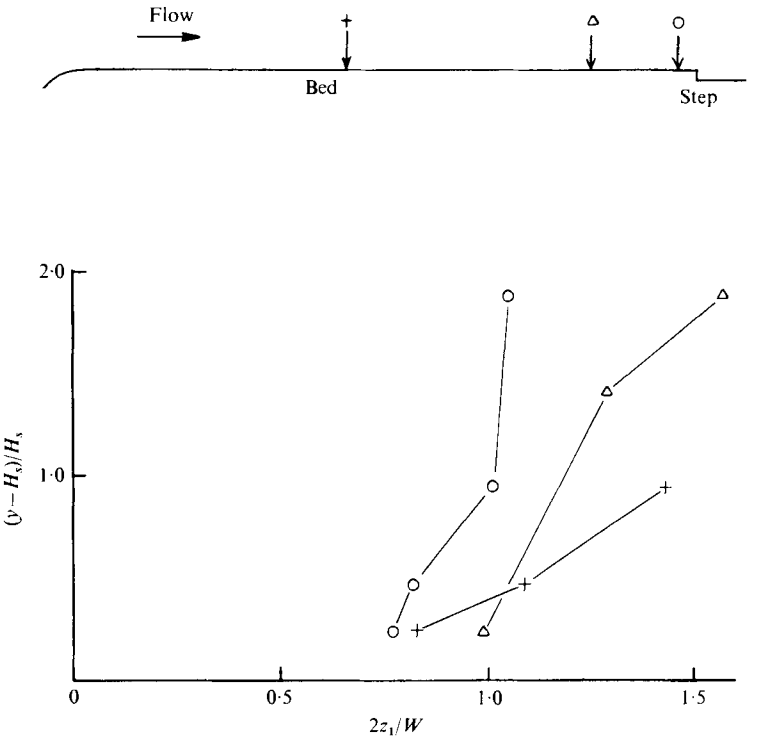

FIGURE 4. Spanwise distance z_1 over which the variation of $\bar{u}/\bar{u}_{max}$ is less than 5 %. ○, $x/H_s = -1{\cdot}71$; △, $x/H_s = -9{\cdot}8$; +, $x/H_s = -31{\cdot}6$.

downstream than $x' = 0{\cdot}44$ m, in order that the shape parameter of the profile would be closer to that of an equilibrium flat-plate profile.

In the second investigation spanwise profiles were measured at several heights above the channel floor at three stations upstream of the step. Figure 4 shows the positions of these stations and gives a summary of the results in the form of plots of $2z_1/W$ against the distance $y - H_s$ from the floor. W denotes the width of the channel and z_1 denotes the spanwise distance from the centre-line for which the variation in $\bar{u}$ is less than 5 % of its value at the centre-line. This method of summarizing the results is made clearer by considering some of the measured spanwise profiles. Figure 5 shows the profiles measured at heights y/H_s of 0·24 and 0·47 above the floor at the streamwise station

$$x/H_s = -1{\cdot}71.$$

The distance x has its origin at the step and is positive in the downstream direction. It can be seen that the profiles are symmetrical about the centre-line. The form of the profiles is consistent with the specific investigation of corner flows described by Mojola & Young (1971). The secondary flows induced by the corner are accompanied by greater distortion of the turbulence field than of the mean streamwise velocity. Figure 4 shows that the extent of two-dimensionality of the $\bar{u}$ profiles increases with the distance y from the wall, whereas the opposite is true for the $(\overline{u'^2})^{\frac{1}{2}}$ profiles (figure 5).

The question that has to be answered is to what extent are the development and the turbulence characteristics of the boundary layer near the centre-line likely to differ

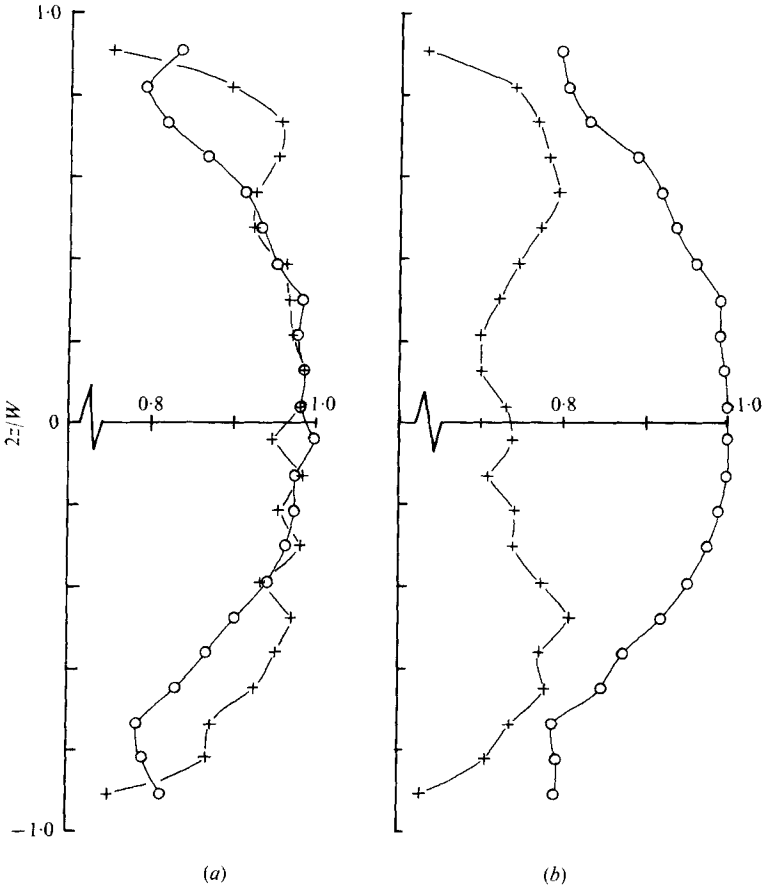

FIGURE 5. Spanwise profiles of $\bar{u}/\bar{u}_{\max}$ (circles) and $10(\overline{u'^2})^{\frac{1}{2}}/\bar{u}_{\max}$ (crosses) measured at two heights at $x/H_s = -1{\cdot}71$. (*a*) $y/H_s = 0{\cdot}236$, (*b*) $y/H_s = 0{\cdot}472$.

from the corresponding boundary layer in a much wider channel. In answering this question two points must be borne in mind. First, the step causes an extremely large perturbation to the layer and the spanwise gradients $\partial/\partial z$ near the centre-line observable in figure 5 are very much smaller than the gradients $\partial/\partial y$ and $\partial/\partial x$ downstream of the step. Second, the results of Mojola & Young show that the wall region of a corner layer settles down to its two-dimensional form within about two layer thicknesses from the corner. In view of this it is considered that, although the overall growth of the present centre-line layer is likely to be affected by the channel side walls, the effect of the side walls on the local turbulence characteristics of the centre-line flow are probably very small in relation to the effect of the step, particularly in the wall region, which is the region of greatest interest.

2.2. *Anemometer system*

Equipment manufactured by DISA formed the basis of the anemometer system.

The optical arrangement of the system is shown in figure 6. It is derived from that described by Oldengarm, van Krieken & Raterink (1973), where the two first-order diffracted beams from a radial diffraction grating form the control volume. Rotation

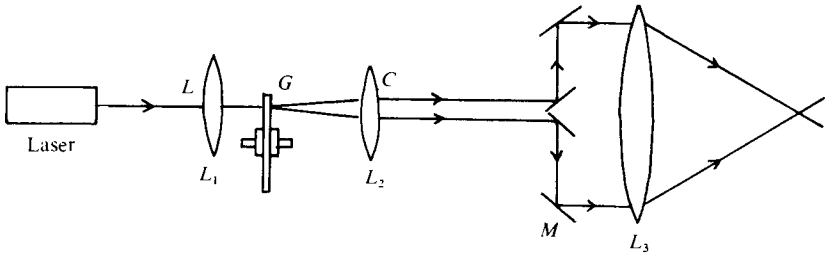

FIGURE 6. Optical arrangement showing grating G, mirror system M and lenses L_1, L_2 and L_3 with focal lengths 127, 330 and 130 mm respectively. LG = 127 mm, GC = 330 mm.

of the grating at a constant speed adds an optical frequency shift (410 kHz), which was essential for the present work.

The arrangement differed from that of Oldengarm *et al.* because it was necessary to increase the angle between the diffracted beams. The angle was smaller than that required since the available grating had a relatively low density of lines, viz. 18·4 lines per mm at the mean track diameter. A periscope system of plane surface-coated mirrors was used to increase the angle.

Signal processing was carried out in the following way. The Doppler signal from a DISA 55L10 Photomultiplier was fed to a DISA 55L20 Doppler Signal Processor, hereafter referred to as the tracker. The output from the tracker was fed to a DISA 55D26 Signal Conditioner where the mean voltage corresponding to the frequency shift was subtracted and the signal was low-pass filtered. Simultaneous measurements of the mean and root-mean-square voltages were obtained from two Solartron JM1860 Analysers using true integration over periods varying from about 1 to 2½ min.

The optical system was mounted on the table of a modified milling machine which allowed accurate traverses to be made in three orthogonal directions. Most of the measurements consisted of traverses through the boundary layer in a direction perpendicular to the bed. The datum position of the control volume was obtained by noting the position at which the control volume was cut by a razor blade at a known height above the bed.

The diffraction grating was driven by a 500 Hz synchronous motor via a simple pulley system. During each traverse the bias voltage corresponding to the frequency shift was monitored.

2.3. *Scope of measurements*

Throughout the report, x denotes the streamwise distance from the face of the step and y denotes the perpendicular distance from the channel bed. The instantaneous velocities in the x and y directions are denoted by u and v respectively, their mean and fluctuating components being denoted by $\bar{u}$ and $\bar{v}$ and u' and v'.

Profiles of $\bar{u}$ and $(\overline{u'^2})^{\frac{1}{2}}$ were measured directly at eight streamwise stations along the channel centre-line. The corresponding values of x/H_s are 0, 1·0, 2·0, 3·0, 4·0, 4·9, 6·0 and 8·26. Similar measurements were made of the velocities at $\pm 45°$ to the x direction in the x, y plane. From these measurements, values of $\bar{v}$, $\overline{u'v'}$ and $\overline{u'^2}+\overline{v'^2}$ were calculated. Values of $\overline{v'^2}/\bar{u}^2_{\max}$ were found by subtracting the directly measured values of $\overline{u'^2}/\bar{u}^2_{\max}$ from the values of $(\overline{u'^2}+\overline{v'^2})/\bar{u}^2_{\max}$ obtained in the above manner.

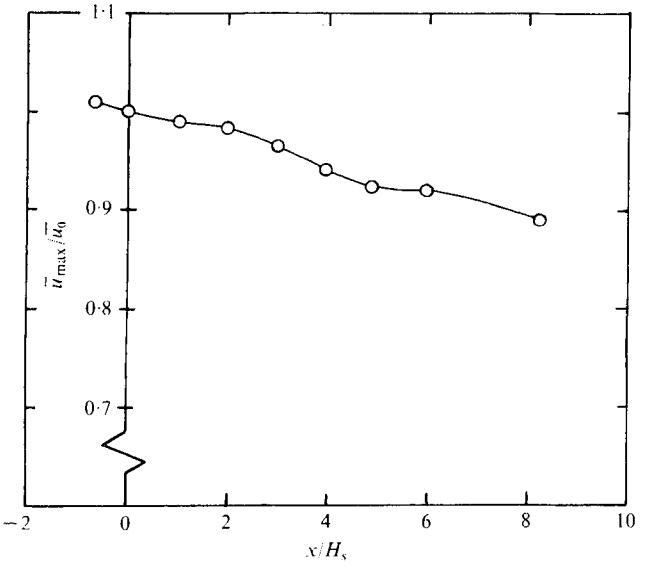

FIGURE 7. Measured streamwise distribution of $\bar{u}_{max}$. $\bar{u}_0 = 276$ mm/s.

A traverse in the streamwise direction was also made to obtain the streamwise variation of $\bar{u}_{max}$, the maximum value of $\bar{u}$ in each velocity profile. Figure 7 shows the measured distribution of $\bar{u}_{max}/\bar{u}_0$, where $\bar{u}_0$ is the value of $\bar{u}_{max}$ at $x/H_s = 0$.

2.4. *Effects of finite control volume*

According to the theory of George & Lumley (1973), which is assumed to be applicable to the present optical arrangement, the spectrum of the velocity indicated by the tracker, $u_t(t)$, say, is a distorted form of the spectrum of the velocity at the centre of the control volume, $u_c(t)$ say.

First, the spectrum of $u_t(t)$ is attenuated at the higher wavenumbers by an extent depending on the relative magnitudes of the width of the control volume and the smaller turbulence scales. Second, the spectrum of $u_t(t)$ suffers from the addition of white noise which corresponds to the ambiguous velocity introduced by the motion of the scattering particles within the control volume. The departures of the spectrum of $u_t(t)$ from that of $u_c(t)$ arise from the combination of the two effects.

The level of the ambiguity noise is determined by the width of the broadening which the ambiguities cause in the spectrum of the Doppler current. Of the various types of broadening only two are of concern here, i.e. transit-time broadening and turbulence broadening. Transit-time broadening is reduced by increasing the diameter of the control volume, whereas turbulence broadening is increased by this action, assuming that the angle θ between the beams is kept constant. Both types of broadening are decreased by increasing θ. The effects of spectral attenuation are reduced at the same time as turbulence ambiguity is reduced. Furthermore the effects of these two phenomena on the measured turbulence power tend to cancel.

Ideally measurements of turbulence intensities should be corrected for both ambiguity noise and spectral attenuation. The corrections for spectral attenuation and

$\frac{1}{2}\theta$ (deg)	e^{-2} × waist diameter (μm)	e^{-2} × width (μm)
10·5	61	330
3·0	38	730

TABLE 1

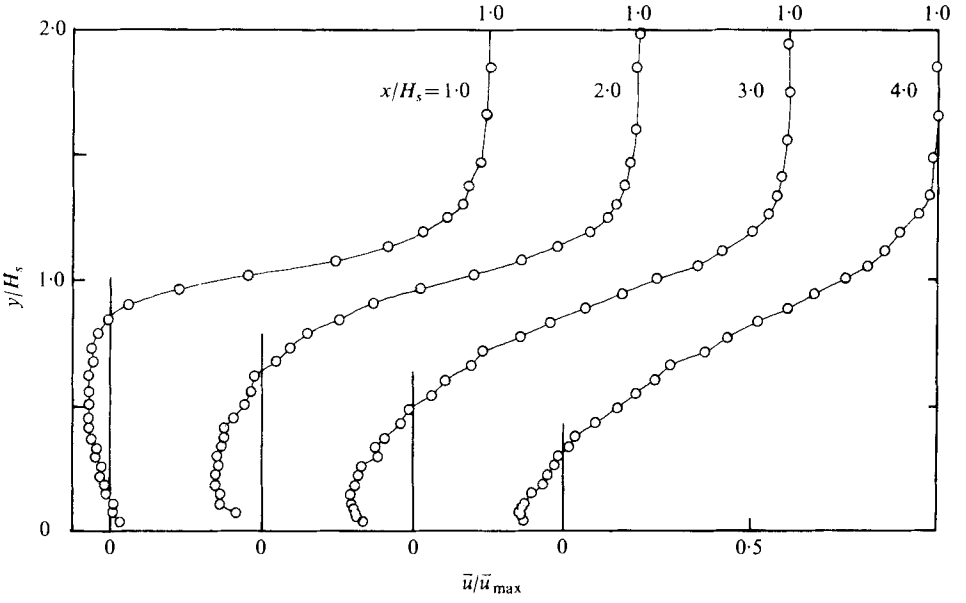

FIGURE 8. Profiles of $\bar{u}/\bar{u}_{max}$ in the separation region.

turbulence ambiguity noise require knowledge of the spectrum of the tracker output and the local dissipation rate ϵ of turbulence energy. This knowledge was not available for the present work, but even if it had been the corrections are only approximate (George & Lumley 1973), since the spectrum of the turbulence is assumed to follow Pao's form.

For the present work, therefore, it was decided to use a fairly large value of $\frac{1}{2}\theta$ to reduce the effects of attenuation and turbulence ambiguity. The calculated dimensions of the control volume are given in table 1.

It was found from measurements in a laminar pipe flow that the noise due to transit-time broadening was negligible, so that corrections were not made for this with $\frac{1}{2}\theta = 10{\cdot}5°$.

A complete test series was also carried out with a different optical arrangement for which $\frac{1}{2}\theta$ was equal to 3·0°. As can be seen from table 1 above, this arrangement was such that all the above effects (transit-time ambiguity, turbulence ambiguity and spectral attenuation) were larger than with the former arrangment. For this reason the results obtained with this arrangement are not presented here. A complete description of these results can be obtained from the authors. In many cases the turbulence profiles obtained with the two optical arrangements are in extremely close agreement

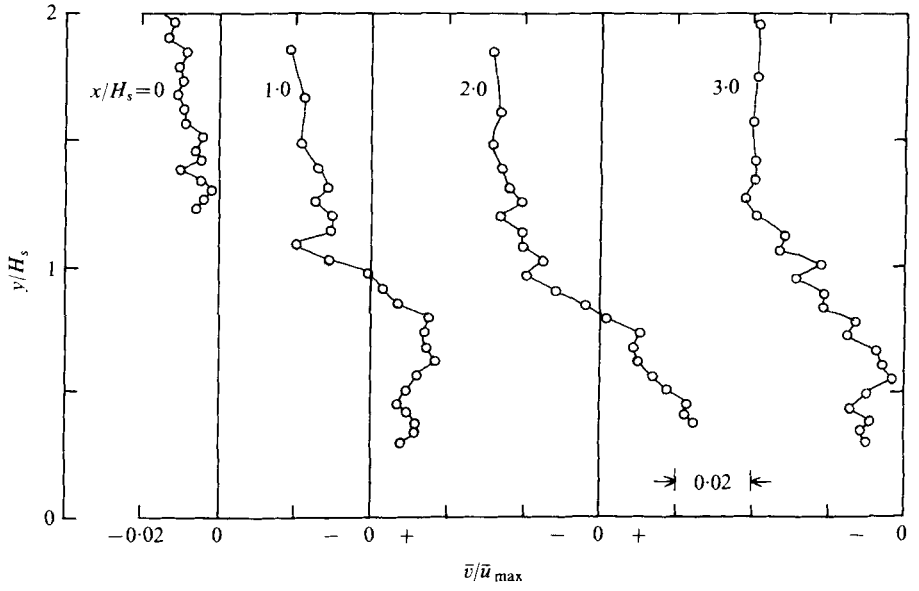

FIGURE 9. Profiles of $\bar{v}/\bar{u}_{max}$ in the separation region.

and are virtually indistinguishable. The largest differences between the two sets of results occur for points lying in or near the separation region. However small differences between the profiles of mean velocity are also apparent in this region and such differences cannot be attributed to the optical arrangement. It is therefore not possible to decide whether the observed differences arise from effects of the finite control volume or from small changes in the flow in the separation regions of the two test series.

3. Results

3.1. *Mean velocity profiles*

The $\bar{u}$ profiles at $x/H_s = 1{\cdot}0$, $2{\cdot}0$, $3{\cdot}0$ and $4{\cdot}0$ are given in figure 8. In their investigations of step flow in a water channel, Abbot & Kline (1962) observed periodicity of very low frequency, of order 1 c/min, in the length of the separated region. Neither of the two main configurations tested by them corresponds exactly to that used here since their steps were situated on the side walls of the channel. However it should be noted that they found the periodicity to be less evident for their single-step configuration (rather than the double-step configuration), which is closest to that of the present work. There was no evidence found during the present measurements of low-frequency oscillations of the mean flow. This was checked by comparing repeat measurements of the profiles. Comparisons were also made between the profiles obtained from direct measurement and the profiles obtained indirectly from the measurements made at $\pm 45°$. Extremely good agreement occurred in all cases and no differences indicative of periodicity were found. If the length of the separated region had been changing with a period of order 1 min this would have manifested itself in a lack of repeatability since the integration times were about 1 min in duration.

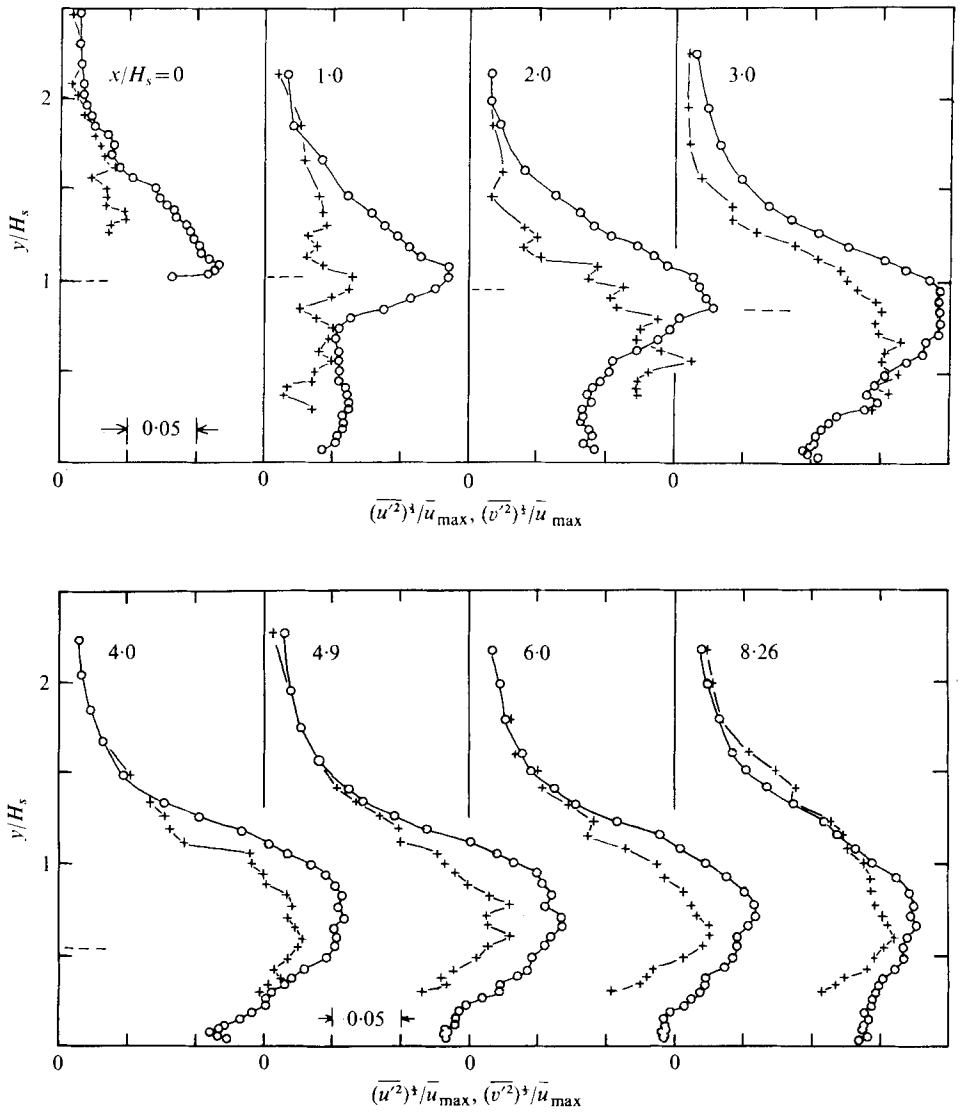

FIGURE 10. Profiles of $\overline{(u'^2)}^{\frac{1}{2}}/\bar{u}_{\max}$ (circles) and $\overline{(v'^2)}^{\frac{1}{2}}/\bar{u}_{\max}$ (crosses). ---, height of the dividing streamline.

Figure 9 shows some of the measured profiles of the mean vertical velocity $\bar{v}$. There is the possibility of large errors in these profiles, because $\bar{v}$ is everywhere very much less than the velocity corresponding to the frequency shift, e.g. in the separation region $\bar{v}$ is typically less than 0·013 times the shift velocity. Furthermore the values of $\bar{v}$ are often obtained by subtracting two large numbers. Nevertheless the profiles are consistent with what one would expect in the separation region. For example, at

$$x/H_s = 1{\cdot}0 \quad \text{and} \quad 2{\cdot}0,$$

$\bar{v}$ changes sign at values of y/H_s of about 1·0 and 0·8 respectively. In figure 12 the mean streamline pattern has been constructed from the $\bar{u}$ profiles which were measured

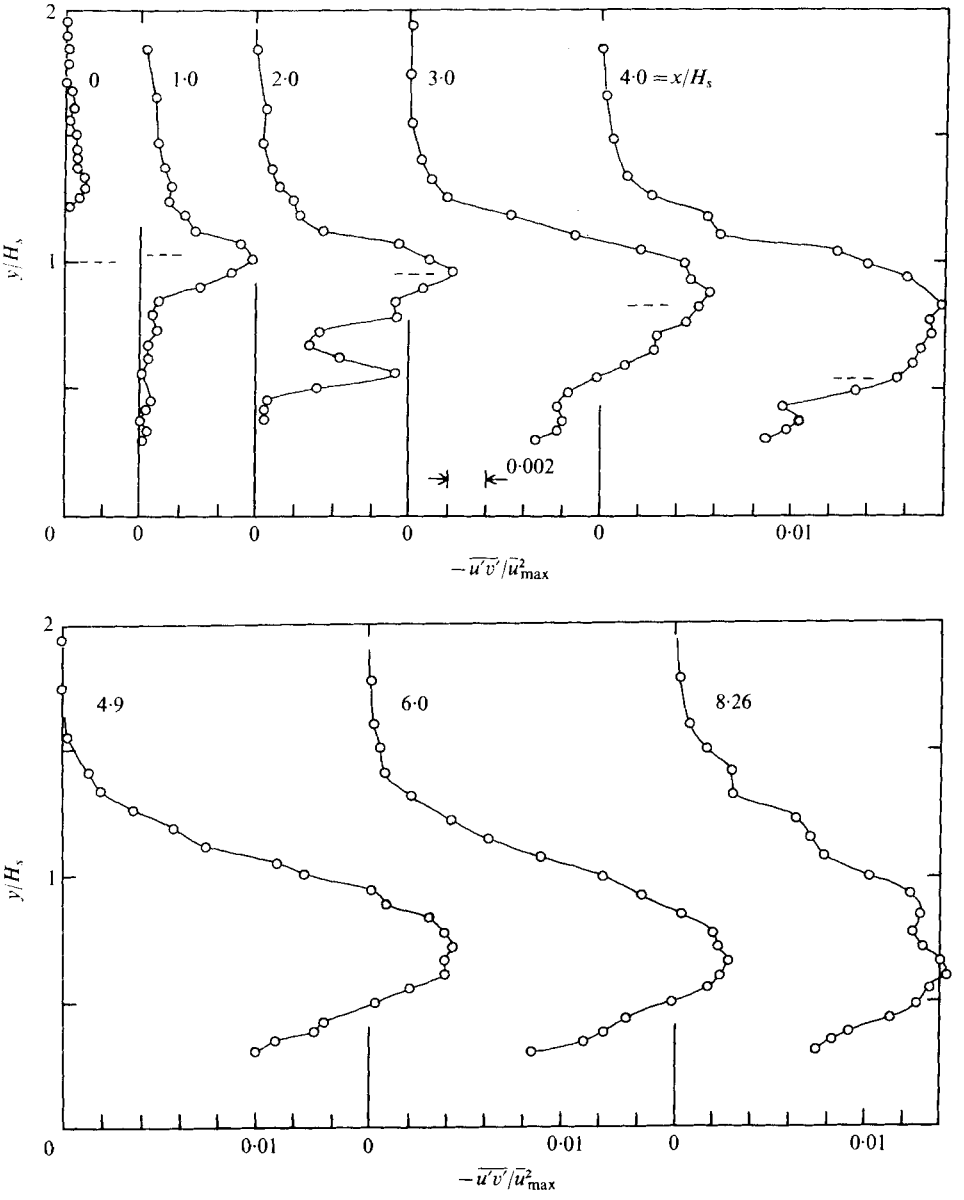

FIGURE 11. Profiles of $-\overline{u'v'}/\bar{u}^2_{\max}$. – – –, height of the dividing streamline.

independently of the $\bar{v}$ profiles. It can be seen that the above two profiles are qualitatively quite consistent with this pattern. When quantitative comparisons were made between the streamline slopes in figure 12 and those calculated from the $\bar{u}$ and $\bar{v}$ profiles it was found that the agreement was generally good.

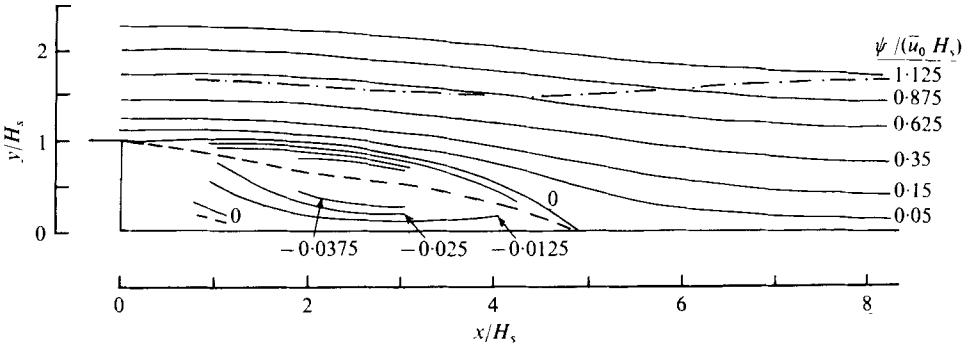

FIGURE 12. Mean non-dimensional streamlines. ----, $\bar{u} = 0$; -·-, $\bar{u}/\bar{u}_{\max} = 0{\cdot}990$.

3.2. *Turbulence profiles*

Figure 10 shows the measured profiles of $(\overline{u'^2})^{\frac{1}{2}}/\bar{u}_{\max}$ and the calculated profiles of $(\overline{v'^2})^{\frac{1}{2}}/\bar{u}_{\max}$. It can be seen that within the region of reverse flow $(\overline{v'^2})^{\frac{1}{2}}$ tends to be as large as or even larger than $(\overline{u'^2})^{\frac{1}{2}}$.

The profiles of $-\overline{u'v'}/\bar{u}^2_{\max}$ are given in figure 11. It is evident that the Reynolds shear stress increases very rapidly with x up to a maximum value of $-\overline{u'v'}/\bar{u}^2_{\max}$ which is about twenty times that at $x/H_s = 0$. It can also be seen that for $x/H_s > 2{\cdot}0$ the shear stress $-\overline{u'v'}$ varies approximately linearly with y for at least part of the profile lying between the wall and the point of maximum shear stress.

4. Analysis of results

4.1. *Mean flow*

Under the assumption of two-dimensional flow, mean streamlines have been constructed from the $\bar{u}$ profiles and these are shown in figure 12 in the form of lines of constant $\psi/(\bar{u}_0 H_s)$, where ψ is the stream function:

$$\psi \equiv \int_0^y \bar{u}\, dy.$$

Figure 12 indicates that the mass flow rate in the reverse-flow region corresponds to a value of $\psi/(\bar{u}_0 H_s)$ of about 0·05. It will be seen later that at reattachment the mass flow rate in the new shear layer is roughly equal to 0·3. Hence on this basis about one-sixth of the new shear layer is deflected upstream.

Semi-logarithmic plots of the $\bar{u}$ profiles downstream of reattachment are given in figure 13. The profiles are shown in the form $\bar{u}/\bar{u}_\tau$ against $\log_{10}(\bar{u}_\tau y/\nu)$ by making use of values of $\bar{u}_\tau$ obtained from the Ludwieg–Tillman relation, i.e.

$$c_f = 0{\cdot}123 \times 10^{-0{\cdot}678H} R_{\delta_2}^{-0{\cdot}268},$$

where $\bar{u}_\tau \equiv \bar{u}_{\max} c_f^{\frac{1}{2}}$ and H and R_{δ_2} are defined below. The fact that the profiles collapse onto the logarithmic line $\bar{u}/\bar{u}_\tau = 5{\cdot}45 + 5{\cdot}5 \log_{10}(\bar{u}_\tau y/\nu)$ with the above values of $\bar{u}_\tau$ could well be fortuitous and no significance can be placed on this. Since no measurements of c_f were made which are independent of the logarithmic-law assumption, there

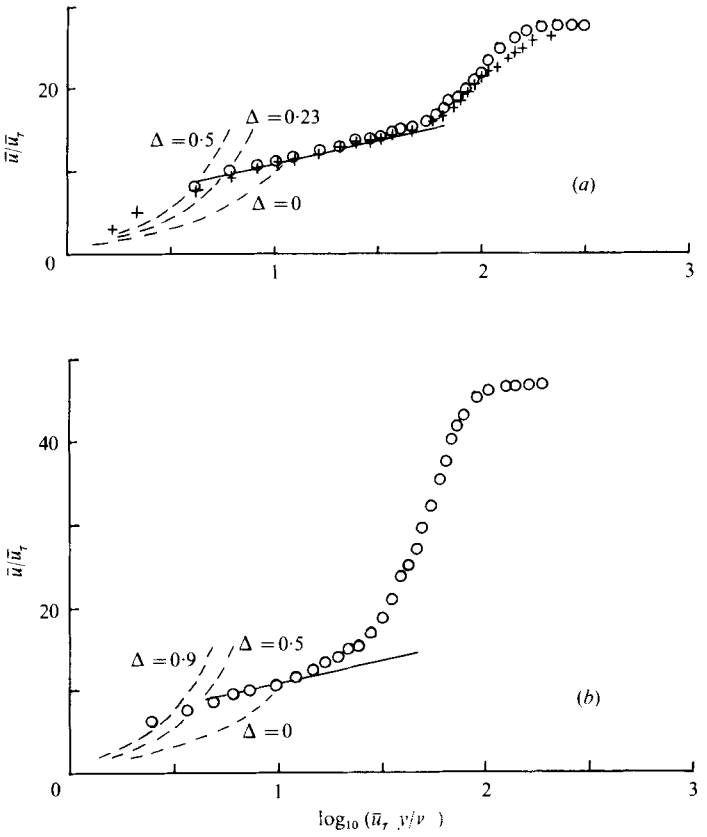

FIGURE 13. Semi-logarithmic plots of $\bar{u}$ profiles downstream of reattachment. ---, $\bar{u}/\bar{u}_\tau = \bar{u}_\tau\, y/\nu$; ——, $\bar{u}/\bar{u}_\tau = 5{\cdot}45 - 5{\cdot}5 \log_{10}(\bar{u}_\tau\, y/\nu)$; +, other optical configuration. (*a*) $x/H_s = 8{\cdot}26$, (*b*) $x/H_s = 6{\cdot}0$.

is no way of deciding whether this law is valid. The plots in figure 13 can in fact be treated as Clauser plots. There is one way of estimating c_f which is independent of the logarithmic law and that is by looking at the velocities measured very close to the wall, i.e. by estimating $(\partial\bar{u}/\partial y)_{y=0}$. This is of course very difficult because the viscous layer will depart from the simple $\bar{u}/\bar{u}_\tau = \bar{u}_\tau\, y/\nu$ form owing to the effect of the relatively very large streamwise pressure gradients in the reattachment region. An expression for this effect, based on the pressure-gradient parameter $\Delta \equiv (\nu/\rho\bar{u}_\tau^3)(\partial p/\partial x)^{-1}$, has been given by Patel (1961), and curves corresponding to different values of Δ are shown in figure 13. The estimated values of Δ for the profiles at $x/H_s = 6{\cdot}0$ and $8{\cdot}26$ are $0{\cdot}9$ and $0{\cdot}23$ respectively (where $\partial p/\partial x$ has been obtained from figure 7 by taking $\partial p/\partial x = -\rho U_e\, \partial U_e/\partial x$) and the corresponding curves are included in figure 13. It can be seen that the measured profiles tend to lie above their respective curves and this indicates that the values of $\bar{u}_\tau$ are underestimated. For $x/H_s = 8{\cdot}26$ the profile measured with the other optical arrangement (see § 2.4 above) is shown since two points are closer to the wall. The good agreement between the two profiles strongly suggests that experimental errors are not significant.

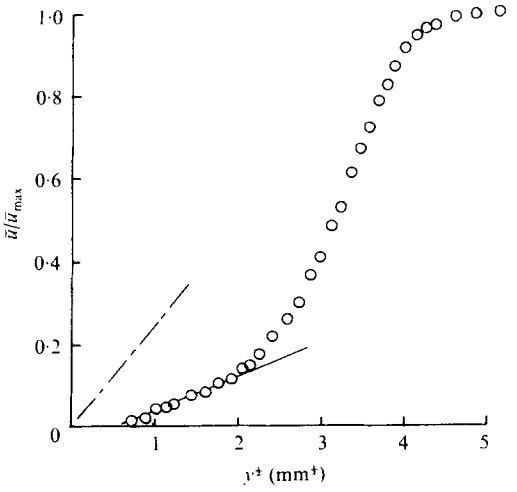

FIGURE 14. Comparison between measured and estimated slopes of $\bar{u}$ profile at reattachment ($x/H_s = 4{\cdot}9$). ———, estimated, $\partial\bar{u}/\partial y^{\frac{1}{2}} = 2\alpha^{\frac{1}{2}}/\bar{u}_{max}k$.

Although we cannot make definitive statements about the profiles in figure 13, they are of interest because Bradshaw & Wong (1972) have discussed in detail the nature of semi-logarithmic plots downstream of reattachment. They describe experimental profiles which exhibit a pronounced drop below the line corresponding to the logarithmic 'law'. Two main possibilities are put forward to explain this behaviour: first, that the turbulence is not in local equilibrium; second, that the length scales of the turbulence near the wall increase more rapidly with y than in a normal equilibrium layer. The large gradient $\partial\bar{\tau}/\partial y$ in shear stress tends to have the opposite effect, but in the profiles of Bradshaw & Wong (1972) this is apparently outweighed by the above two effects. For the present profiles there is no evidence of a drop below the logarithmic line and it seems that this reflects the fact that these profiles were measured closer to reattachment. The profile of Bradshaw & Wong measured furthest upstream is that at $x/H_s = 10$. This implies that the ratio $(y\,\partial\bar{\tau}/\partial y)\,\bar{\tau}_w^{-1}$, which is a rough measure of the opposing effect, decreases very rapidly downstream of reattachment ($\bar{\tau}_w$ denotes the wall value of the mean shear stress $\bar{\tau}$).

There is positive evidence of a more rapid increase in the mixing length l near the wall when one considers the profile at $x/H_s = 4{\cdot}9$. This profile lies very close to the reattachment point, where $\bar{\tau}_w = 0$, and one can expect $\bar{u}/\bar{u}_{max}$ to be proportional to $y^{\frac{1}{2}}$ with a slope given by $2\alpha^{\frac{1}{2}}/(\bar{u}_{max}\,k)$, where $\alpha \equiv \partial(-\overline{u'v'})/\partial y$ and k is the von Kármán constant in $l = ky$. The expression for the slope follows from Townsend's (1961) equation (4.2) when the effects of gradient diffusion are neglected. It can also be derived by assuming that $\bar{\tau}$ increases linearly with y, in a similar way to Stratford (1964), i.e. by assuming $\bar{\tau} = y\,\partial\bar{\tau}/\partial y$ for $\bar{\tau}_w = 0$ and y small. This assumption certainly seems to be justified by the measured shear-stress profile at $x/H_s = 4{\cdot}9$ (figure 11), although the measurements do not extend close enough to the wall to be conclusive. Figure 14 shows both the profile plotted as $\bar{u}/\bar{u}_{max} \sim y^{\frac{1}{2}}$ and the slope of the line given by the above expression, where k has been taken as 0·41 and α has been calculated from figure 11. The measured profile is approximately linear in the wall region, but the slope is much

x/H_s	δ_2 (mm)	δ_1 (mm)	H	R_{δ_2}	c_f	$\overline{u}_\tau/\overline{u}_{\max}$
1·0	0·65	15·0	23·1	156·5	0	0
2·0	0·69	14·3	20·8	169·4	0	0
3·0	0·88	13·0	14·9	213·2	0	0
4·0	1·81	11·3	6·3	439·6	0·00001	0·0012
4·9	2·72	9·8	3·6	646·0	0·00008	0·0089
6·0	3·35	8·2	2·44	753·6	0·00046	0·0214
8·26	3·47	6·1	1·77	772·6	0·00131	0·0362

$$\delta_2 \equiv \int_0^\delta \overline{u}(\overline{u}_{\max} - \overline{u})\, dy/\overline{u}_{\max}^2, \quad H \equiv \frac{\delta_1}{\delta_2},$$

$$\delta_1 \equiv \int_0^\delta (\overline{u}_{\max} - \overline{u})\, dy/\overline{u}_{\max}, \quad R_{\delta_2} \equiv \frac{\overline{u}_{\max}\,\delta_2}{\nu}.$$

TABLE 2

less than the calculated slope, and this is consistent with an increased value of k in the measured profile. A value of about unity would give good agreement. It is concluded therefore that, although the concept of a mixing length increasing linearly with y near the wall is compatible with the present measurements, the rate of increase is over twice the von Kármán constant.

This conclusion is unlikely to be significantly affected by errors in the $\overline{u}$ measurements, because these would have to be serious and there is definitely no evidence of this either from the repeatability checks or from the measurements made with the other optical arrangement. The only significant source of error lies in the estimation of $\partial\overline{\tau}/\partial y$ from the measured shear-stress profile in figure 11. The measured points do indicate that the gradient can be considered constant in the wall region, but one cannot be absolutely certain of this. However, it is possible to obtain an independent estimate of $\partial\overline{\tau}/\partial y$ at $y = 0$ from figure 7. At the wall, the streamwise pressure gradient $\partial p/\partial x$ is equal to $\partial\overline{\tau}/\partial y$ and we can also take $\partial p/\partial x \doteq -\rho U_e\,\partial U_e/\partial x$ because the pressure gradient due to the change in height of the free surface is small (the theoretical change in height of the free surface measured from the channel bed, which was made horizontal with a clinometer, is only 0·36 mm). The value of the shear-stress gradient at the wall estimated from figure 11 is 0·20 N/m^3, which compares very favourably with the value of 0·24 N/m^3 for the gradient away from the wall measured from figure 7.

Further evidence of a larger rate of increase of l with y will be seen in the actual profiles of the mixing length given below.

The properties of the $\overline{u}$ profiles are summarized in table 2.

4.2. *Turbulence profiles*

Bradshaw & Wong (1972) describe a new shear layer whose length scales, downstream of reattachment at least, differ considerably from those of a plane mixing layer. More specifically, the mixing length $l \equiv (\tau/\rho)^{\frac{1}{2}}(\partial\overline{u}/\partial y)^{-1}$ is a larger multiple of x than is the case in a plane mixing layer, whereas there is evidence that the dissipation length scale $L \equiv (-\overline{u'v'})^{\frac{3}{2}}/\epsilon$ is a smaller multiple of x.

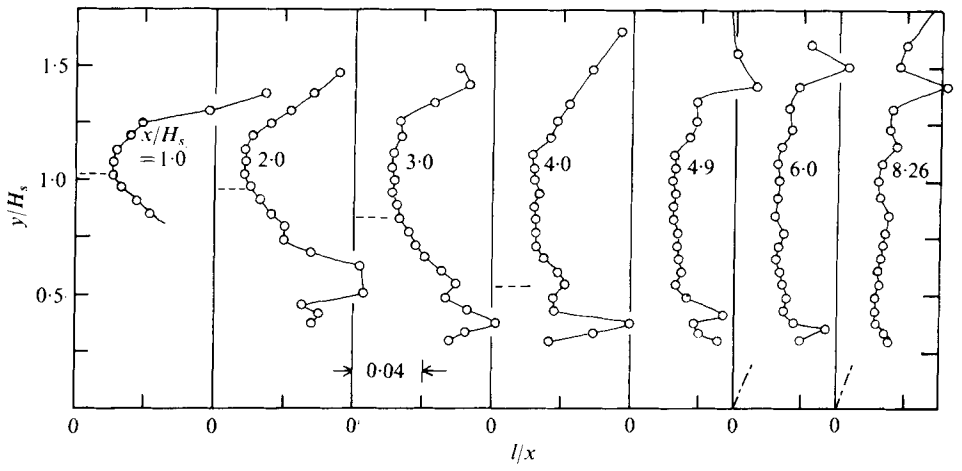

FIGURE 15. Profiles of the mixing-length ratio l/x. ---, height of the dividing streamline; -·-·-, $l = 0{\cdot}41y$.

From the present results it has been possible to evaluate the profiles of the mixing length and these are given in figure 15 in the form l/x against y. The gradient $\partial\overline{u}/\partial y$ has been estimated from

$$\left[\frac{\partial u}{\partial y}\right]_i = \frac{1}{2}\left(\frac{\overline{u}_{i+1}-\overline{u}_i}{y_{i+1}-y_i} - \frac{\overline{u}_i-\overline{u}_{i-1}}{y_i-y_{i-1}}\right),$$

where the subscripts $i-1$, i and $i+1$ denote consecutive measurement points. Large errors in $\partial\overline{u}/\partial y$ can be expected in the outer region of the flow, where $\partial\overline{u}/\partial y$ is small. However, in this region l/x shows a distinct tendency to increase with y and this is to be expected since the mixing length in the outer region of the boundary layer upstream of the step should follow the normal relationship, i.e. $l \doteq 0{\cdot}09\delta$, where δ is the boundary-layer thickness. Hence at $x/H_s = 1{\cdot}0$, say, the value of l/x in that part of the outer region which is unaffected by the new shear layer will be about 0·10, which compares favourably with the results in figure 15.

Viewed as a whole, the mixing-length profiles are consistent with the development of a new shear layer, identified by a region of constant l/x whose width initially increases as x increases. The value of l/x in this region is about 0·025, which lies within the range of values cited by Bradshaw & Wong (1972). Within the separation bubble l/x tends to large values (at $x/H_s = 1{\cdot}0$ and 2·0, $\partial\overline{u}/\partial y$ tends to zero) but here l is not a meaningful measure of the turbulence length scale. For the reattachment profile and the two downstream profiles the linear relation $l = 0{\cdot}41y$ is shown and it can be inferred that there is a region near the wall where l increases more rapidly than this with y. The measurements indicate in fact that as the wall is approached l passes through a maximum before decreasing to zero. This behaviour can be observed in some length-scale predictions given by Launder & Spalding (1972) for a similar but not identical step configuration. The predicted length scale, denoted here by l_1, is not the mixing length l, although it is related to it by $l_1 = l(-\overline{u'v'})^{\frac{1}{2}}/e^{\frac{1}{2}}$, where e denotes $\frac{1}{2}(\overline{u'^2}+\overline{v'^2}+\overline{w'^2})$. Profiles of l_1 have been evaluated from the measurements and are given in figure 16. Since $\overline{w'^2}$ was not measured it has been assumed that e can be taken as $\frac{3}{4}(\overline{u'^2}+\overline{v'^2})$. As

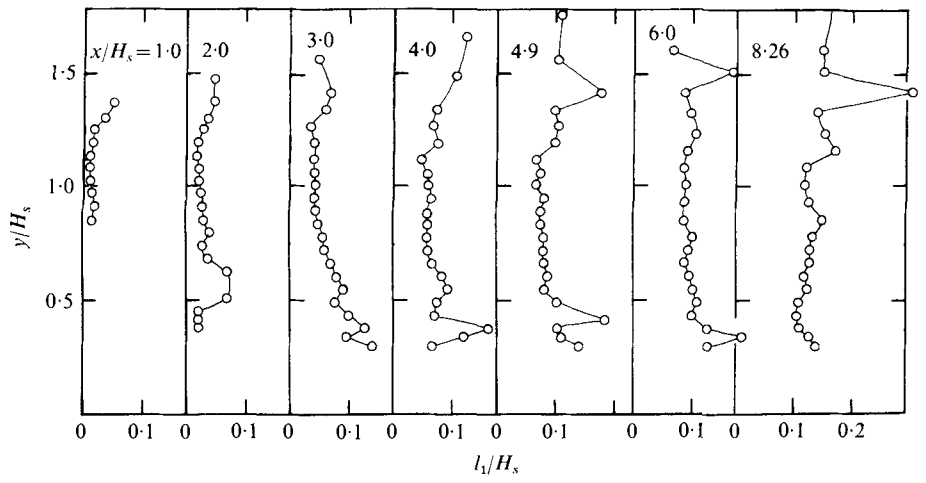

FIGURE 16. Profiles of the length-scale ratio l_1/H_s.

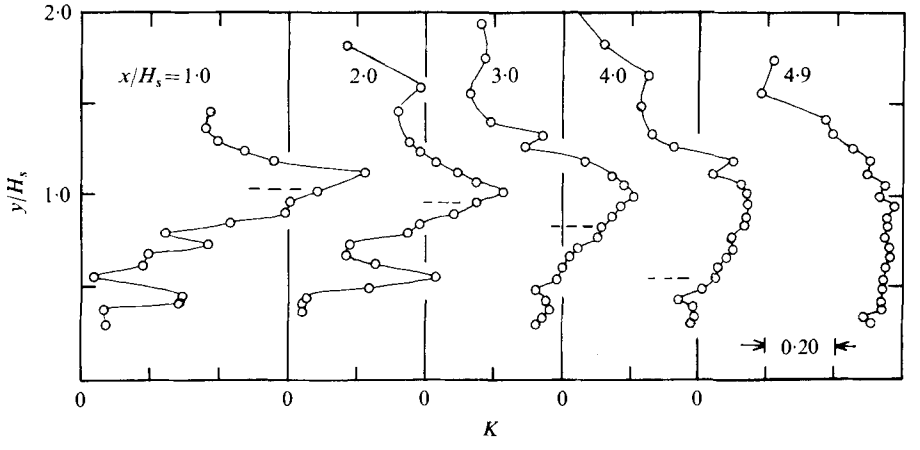

FIGURE 17. Profiles of the shear correlation coefficient K. ---, height of the dividing streamline.

with the profiles of l, scatter can be expected to be present in the l_1 profiles because $\partial\overline{u}/\partial y$ is required for the evaluation. Nevertheless it can still be deduced that a maximum occurs in the profiles, particularly at $x/H_s = 3{\cdot}0$.

The development of the new shear layer can also be distinguished in the profiles of the shear correlation coefficient $K \equiv -\overline{u'v'}/(\overline{u'^2})^{\frac{1}{2}}(\overline{v'^2})^{\frac{1}{2}}$, given in figure 17. At the station $x/H_s = 1{\cdot}0$ a definite peak occurs in the K profile at a value of y which is close to the position of the dividing streamline. This peak is still clearly apparent in the profiles at $x/H_s = 2{\cdot}0$ and $3{\cdot}0$, but at the latter station the profile has become noticeably fuller in the vicinity of the peak. At $x/H_s = 4{\cdot}0$ a peak is no longer visible and by $x/H_s = 4{\cdot}9$ the profile has a flat appearance with K approximately constant and equal to $0{\cdot}55$. This region of constant K is apparent in the remaining profiles. If one takes the outer boundary of the new shear layer to correspond to $K = 0{\cdot}55$, then this boundary lies at $y \simeq 1{\cdot}05H_s$ at $x/H_s = 4{\cdot}9$, which corresponds to the value $\psi/(\overline{u}_0 H_s) \simeq 0{\cdot}3$ in figure 12 referred to in §4.1.

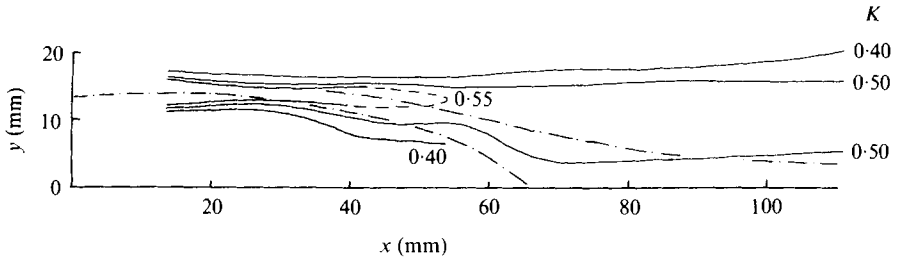

FIGURE 18. Lines of constant shear correlation coefficient. ——, streamlines $\psi/(\bar{u}_0 H_s) = 0$ and 0·10.

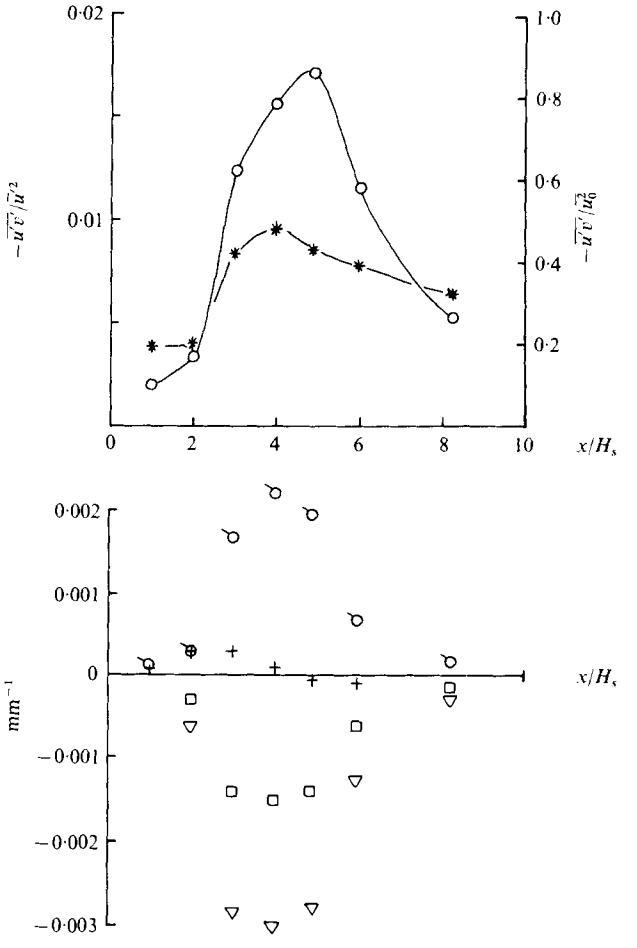

FIGURE 19. Development of $-\overline{u'v'}/\bar{u}_0^2$ along the streamline $\psi/(\bar{u}_0 H_s) = 0{\cdot}10$:

○, $-\overline{u'v'}/\bar{u}_0^2$; ⟍○, $\dfrac{\overline{v'^2}}{\bar{u}_0^3}\dfrac{\partial\bar{u}}{\partial y}+\dfrac{\overline{u'^2}}{\bar{u}_0^3}\dfrac{\partial\bar{v}}{\partial x}+\dfrac{\overline{u'v'}}{\bar{u}_0^3}\dfrac{\partial\bar{v}}{\partial y}+\dfrac{\overline{u'v'}}{\bar{u}_0^3}\dfrac{\partial\bar{u}}{\partial x}$; +, $\dfrac{(\bar{u}^2+\bar{v}^2)^{\frac{1}{2}}}{\bar{u}_0^3}\dfrac{\partial(-\overline{u'v'})}{\partial s}$;

□, $\dfrac{\epsilon}{\bar{u}_0^3}=\dfrac{(-\overline{u'v'}/\bar{u}_0^2)^{\frac{3}{2}}}{0{\cdot}024x}$; ▽, $\dfrac{\epsilon}{\bar{u}_0^3}=\dfrac{(-\overline{u'v'}/\bar{u}_0^2)^{\frac{3}{2}}}{0{\cdot}012x}$;

*, development of $-\overline{u'v'}/\overline{u'^2}$.

The behaviour of K in the reattachment region is of particular interest, because in this region one can expect changes in the shape of turbulence spectra to be significant. If as reattachment is approached there is a shift of energy to higher wavenumbers, corresponding to a reduction in eddy size, then one might expect a reduction in K. This follows from the expectation that a greater proportion of $-\overline{u'v'}$ lies in the large eddies than is the case for $\overline{u'^2}$ and $\overline{v'^2}$, so that a shift of energy to the higher wavenumbers is accompanied by a reduction in K. Figure 18 shows lines of constant K in relation to the mean streamlines $\psi/(\bar{u}_0 H_s) = 0$ and 0·10. There is a decrease in K along streamlines entering the reattachment region, but this is not greatly in evidence further downstream. The results show a region in which K is of similar magnitude to that observed in a plane mixing layer ($K \simeq 0{\cdot}6$ in Townsend 1956, p. 179) and which is apparently unaffected by the reattachment region. To this extent the present results do not support the description of a shear layer with a much reduced length scale relative to that in a plane mixing layer.

Bradshaw & Wong (1972) also suggested that the supposed reduction in turbulence length scale manifests itself as a rapid decrease in shear stress downstream of reattachment. Figure 19 shows the development of $-\overline{u'v'}/\bar{u}_0^2$ along the streamline

$$\psi/(\bar{u}_0 H_s) = 0{\cdot}10,$$

which is quite close to the locus of maximum shear stress. The rapid decrease in $-\overline{u'v'}/\bar{u}_0^2$ after reattachment is evident, but there is also a large decrease in the production term, to which $\overline{v'^2}(\partial\bar{u}/\partial y)\bar{u}_0^{-3}$ makes by far the largest contribution. Also shown in the figure are the values of the dissipation term corresponding to

$$L = 0{\cdot}012x \quad \text{and} \quad L = 0{\cdot}024x,$$

which have been evaluated by assuming that the relation $\epsilon = (-\overline{u'v'})^{\frac{3}{2}}/L$ is valid. Of these two expressions for L, the former is that tentatively suggested by Bradshaw & Wong (1972) and the latter is that quoted by them for a plane mixing layer. Simply comparing the difference between the production and advection terms with the two dissipation terms indicates that, up to $x/H_s \simeq 3{\cdot}0$, $L = 0{\cdot}024x$ gives the better estimate of the length scale. For $x/H_s > 3{\cdot}0$ the best estimate appears to lie somewhere between the two expressions. The pressure transport and convective diffusion terms have of course been neglected in the above comparison and it is not possible to say with certainty how their magnitude and sign vary along $\psi/(\bar{u}_0 H_s) = 0{\cdot}10$, so no definite conclusions can be drawn.

The components of the rates of strain estimated from the mean velocity profiles are given in figure 20. It can be seen that $\partial\bar{u}/\partial x$ becomes significant in relation to $\partial\bar{u}/\partial y$. For a truly two-dimensional flow $\partial\bar{u}/\partial x = -\partial\bar{v}/\partial y$ (so the estimates indicate that departures from two-dimensionality are small), and the production of $-\overline{u'v'}$ will not be directly affected by this but the distribution of energy between the normal stresses will be modified.

One of the referees has pointed out that rapid-distortion theories like those discussed by Townsend (1970) and Hunt (1973) can give qualitative insight into some of the present observations. For this purpose we consider the distortion of vortex lines which move with the mean flow. Thus a vortex line such as AB in figure 21 is rotated and stretched to $A'B'$ by the rate of strain $\partial\bar{u}/\partial y$. The calculations of Townsend for the case

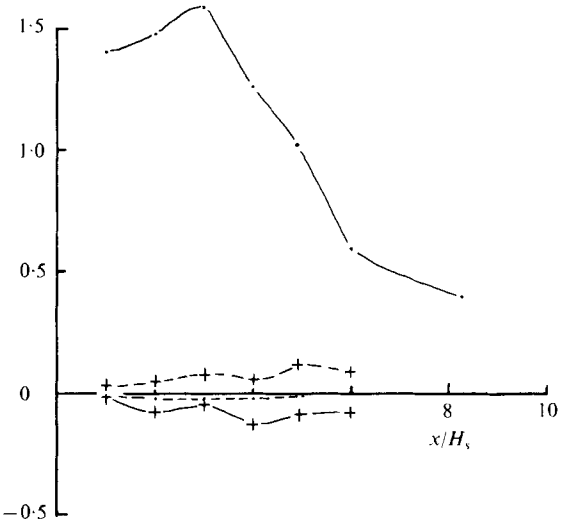

FIGURE 20. Mean rates of strain along the streamline $\psi/(\bar{u}_0 H_s) = 0{\cdot}10$. ·—·, $H_s(\partial\bar{u}/\partial y)\,\bar{u}_0^{-1}$; ·––·, $H_s(\partial\bar{v}/\partial x)\,\bar{u}_0^{-1}$; +—+, $H_s(\partial\bar{v}/\partial y)\,\bar{u}_0^{-1}$; +––+, $H_s(\partial\bar{u}/\partial x)\,\bar{u}_0^{-1}$.

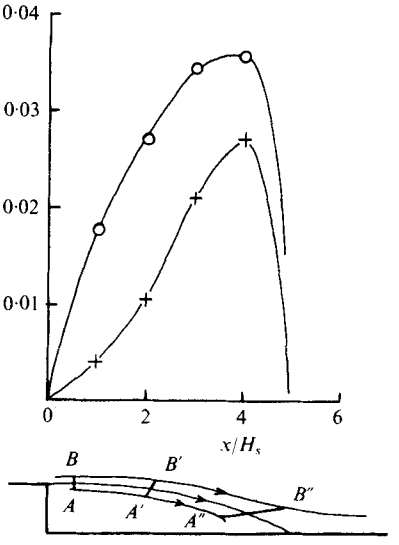

FIGURE 21. Development of $\overline{u'^2}$ (circles) and $\overline{v'^2}$ (crosses) along dividing streamline.

of initially homogeneous turbulence show how a high shear stress $-\overline{u'v'}$ results from this distortion. In particular, it is shown that the ratio $-\overline{u'v'}/\overline{u'^2}$ rapidly reaches a peak, followed by a slow decline. Similar behaviour can be observed in the present results plotted in figure 19.

As the vortex line approaches the wall ($A''B''$ in figure 21), the situation becomes similar to that near a stagnation line, which has been discussed by Hunt. The effect of blocking by the surface becomes important and tends to reduce $\overline{v'^2}$ while increasing $\overline{u'^2}$ and $\overline{w'^2}$. The stretching due to the longitudinal strain $\partial\bar{u}/\partial x$ has the effect of

increasing $\overline{v'^2}$ and $\overline{w'^2}$ at the expense of $\overline{u'^2}$. These two effects act on the energy contained in the larger and smaller scales to different degrees. Their combined effect is more likely to be apparent along the dividing streamline and figure 21 shows the measured development of $\overline{u'^2}$ and $\overline{v'^2}$ along $\psi/(u_0 H_s) = 0$. It can be seen that as reattachment is approached $\overline{u'^2}$ starts to decrease sooner than $\overline{v'^2}$, so that the effect of distortion appears to be more significant than blocking until quite close to the surface.

5. Conclusions

The considerable differences which are apparent between the present results and those described by Raudkivi (1963) are thought to be due to the different measurement techniques.

Examination of the mean velocity profile $\bar{u} \sim y$ at reattachment indicates strongly that the length scale near the wall increases with y at about twice the rate for a normal attached boundary layer. Further evidence of this can be seen in the profiles of the mixing length l and a similar length scale l_1. These profiles also indicate that the scales pass through a maximum near the wall. Semi-logarithmic plots of the $\bar{u}$ profiles immediately downstream of reattachment do not exhibit the behaviour which has been observed by other investigators, but this probably reflects the proximity of the present profiles to reattachment, where the shear-stress gradient $\partial\bar{\tau}/\partial y$ is very large.

The turbulence measurements have revealed the development of a new shear layer, which splits at reattachment with about one-sixth of the mass flow deflected upstream. The new shear layer is associated with a region of roughly constant values of l/x and K. Large values of $-\overline{u'v'}$ occur in the layer, a maximum value of about twenty times that in the upstream layer occurring at a streamwise position close to reattachment. Downstream of reattachment $-\overline{u'v'}$ decreases very rapidly. In the reverse-flow region $-\overline{u'v'}$ is also generally large and increases linearly with y over at least part of this region.

The mixing-length ratio l/x is larger than that found in plane mixing layers, but conclusions about the size of the dissipation length scale L are very tenuous. The shear correlation coefficient K has a level which is about the same as that found in plane mixing layers, and there are no sudden changes in K over much of the shear layer downstream of reattachment. Investigation of the development of $-\overline{u'v'}$ along a mean streamline indicates that much of the rapid decrease in $-\overline{u'v'}$ is due to a decrease in the shear-stress production term, although there is some evidence of a simultaneous decrease in the length-scale ratio L/x. The fact that there is not a great deal of evidence of large changes in K and L/x over much of the shear layer downstream of reattachment is consistent with the observation that only a small fraction of the shear layer is deflected upstream.

REFERENCES

ABBOT, D. E. & KLINE, S. J. 1962 *Trans. A.S.M.E., J. Basic Engng* **84**, 317.
BRADSHAW, P. & WONG, F. Y. F. 1972 *J. Fluid Mech.* **52**, 113.
GEORGE, W. K. & LUMLEY, J. L. 1973 *J. Fluid Mech.* **60**, 321.
GRANT, I., BARNES, F. H. & GREATED, C. A. 1975 *Phys. Fluids* **18**, 504.

HUNT, J. C. R. 1973 *J. Fluid Mech.* **61**, 625.

LAUNDER, B. E. & SPALDING, D. B. 1972 *Mathematical Models of Turbulence.* Academic Press.

MOJOLA, O. O. & YOUNG, A. D. 1971 *AGARD Conf. Turbulent Shear Flows, London, AGARD Conf. Proc.* no. 93–71.

OLDENGARM, J., VAN KRIEKEN, A. H. & RATERINK, H. J. 1973 *Optics Laser Tech.* **5** (6), 249.

PATEL, V. C. 1961 *J. Fluid Mech.* **11**, 185.

RAUDKIVI, A. J. 1963 *J. Hyd. Div., Proc. A.S.C.E.* **89** (HY6), 15.

STRATFORD, B. 1964 *J. Fluid Mech.* **5**, 1.

TOWNSEND, A. A. 1956 *The Structure of Turbulent Shear Flow.* Cambridge University Press.

TOWNSEND, A. A. 1961 *J. Fluid Mech.* **11**, 97.

TOWNSEND, A. A. 1970 *J. Fluid Mech.* **41**, 13.